

引文格式: 徐刚, 薛涛, 胡彦华, 等. 喷丸覆盖率对 2024-T351 铝合金表面完整性的影响[J]. 航空制造技术, 2024, 67(13): 106-112.
XU Gang, XUE Tao, HU Yanhua, et al. Effect of shot peening coverage on surface integrity of 2024-T351 aluminum alloy[J].
Aeronautical Manufacturing Technology, 2024, 67(13): 106-112.

喷丸覆盖率对 2024-T351 铝合金表面完整性的影响

徐刚¹, 薛涛¹, 胡彦华¹, 肖雄¹, 曹一², 张琪²

(1. 中航西安飞机工业集团股份有限公司, 西安 710089;

2. 西北工业大学, 西安 710072)

[摘要] 喷丸覆盖率对零件的服役性能具有十分重要的影响。本文以 2024-T351 铝合金作为研究对象, 通过调整喷丸进给速度获得 4 种喷丸覆盖率: 88.3%、100%、200%、400%。使用扫描电子显微镜、粗糙度仪、残余应力分析仪、微观硬度计等研究了喷丸覆盖率对表面形貌、表面粗糙度、残余应力和微观硬度的影响。随着喷丸覆盖率的增加, 试样表面粗糙度先升高后下降。100% 覆盖率的喷丸试样表面粗糙度 R_a 达到最大值 4.601 μm 。在 400% 的覆盖率下, 试样表面出现较多的褶皱及微裂纹。喷丸覆盖率的增加导致残余压应力最大值的提高和残余应力场深度的增大。喷丸试样的微观硬度和硬化层深度随覆盖率的增加而增大, 对应于 88.3%、100%、200% 和 400% 覆盖率的喷丸试样表面微观硬度分别增加了 18.4%、22.8%、25.1%、27.2%。

关键词: 喷丸覆盖率; 表面完整性; 表面粗糙度; 残余应力; 微观硬度

Effect of Shot Peening Coverage on Surface Integrity of 2024-T351 Aluminum Alloy

XU Gang¹, XUE Tao¹, HU Yanhua¹, XIAO Xiong¹, CAO Yi², ZHANG Qi²

(1. AVIC Xi'an Aircraft Industry Group Company Ltd., Xi'an 710089, China;

2. Northwestern Polytechnical University, Xi'an 710072, China)

[Abstract] Peening coverage has essential effects on the service performance of parts. In this paper, aluminum alloy 2024-T351 was subjected to pneumatic shot peening with different coverage of 88.3%, 100%, 200% and 400% by adjusting feeding speed. The surface topography and microstructure, roughness, residual stress and microhardness were investigated using a scanning electron microscope, roughness tester, residual stress instrument and Vickers hardness tester. The surface roughness increases first and then decreases with the increase of peening coverage. The average surface roughness of peened sample with 100% coverage is 4.601 μm , which is the highest value. Moreover, the peened surface shows significant folds and microcracks owing to the high coverage of 400%. The increase of peening coverage leads to the enlargement of the maximum compressive residual stress and depth of the compressive residual stress layer. Similarly, the maximum hardness and hardened layer depth are enhanced with peening coverage. The maximum hardness corresponding to peening coverage of 88.3%, 100%, 200% and 400% is increased by 18.4%, 22.8%, 25.1% and 27.2%, respectively.

Keywords: Shot peening coverage; Surface integrity; Surface roughness; Residual stress; Microhardness

DOI: 10.16080/j.issn1671-833x.2024.13.106

2024-T351 铝合金因其密度低、比强度高、耐腐蚀性好等优点, 广泛应用于航空航天领域^[1-3]。在零件的服役过程中, 疲劳、腐蚀及磨损等不同类型的失效通常起源于材料表面, 因此, 需要合适的表面处理工艺来提

高其综合性能。喷丸是一种常见且高效的表面处理工艺, 可以有效提高材料的表面性能^[4-6]。然而, 喷丸覆盖率的不同引起的材料表面完整性的变化将造成零件综合性能的差异^[7]。因此, 研究喷丸覆盖率对表面完整性

的影响具有十分重要的意义。

在喷丸过程中,大量弹丸撞击材料表面引起微观结构演变,包括晶粒细化^[8]、位错增殖、残余应力^[9]、粗糙度增加^[10]等,进而影响材料的综合性能。常用的喷丸方法包括气动喷丸^[11]、超声喷丸^[12]、激光喷丸^[13]、空化喷丸^[14]等,已被应用于钛合金^[15]、铝合金^[16]、镁合金^[17]和不锈钢^[18]等材料的表面强化。在晶粒细化方面,Liu等^[19-20]研究了高能气动喷丸对TC4钛合金微观结构的影响,指出位错运动及其演化主导了 α Ti纳米晶的形成,而孪晶和相变在晶粒细化过程中起辅助作用。Li等^[21]同样指出高能喷丸TC17钛合金晶粒细化机制为位错运动。Ao等^[22-23]利用超声滚压在TC4钛合金表面制备出纳米晶-超细晶-细晶-粗晶的梯度纳米结构。由于晶粒细化、晶格畸变、位错增殖等,材料表层的硬度明显增大,耐磨损性提高^[24-25]。Zhang等^[26]发现喷丸产生的纳米晶抑制了AZ31镁合金在磨损过程中材料的软化和熔化,磨损量显著降低。相比于原始试样,喷丸处理后的17Cr2Ni2MoVNB钢具备较低的摩擦系数和较好的耐磨损性^[27]。而喷丸产生的残余压应力场可以有效延缓零件表面裂纹萌生,减小裂纹扩展速率,有利于疲劳寿命的提高^[28-31]。Luo等^[32]指出,位错强化、残余应力和晶粒细化的协同作用可使喷丸强化的TC4钛合金疲劳寿命显著提高。然而,不恰当的喷丸参数会导致表面粗糙度显著增加,甚至引起表面微裂纹萌生,对疲劳性能产生不利影响^[33-34]。Gao等^[35]研究发现,喷丸造成的较深凹坑和微裂纹等缺陷降低了材料的超高周疲劳寿命。Liu等^[36]指出抛光处理降低了喷丸试样的表面粗糙度,显著提高了试样的疲劳性能。

覆盖率作为喷丸强化的重要参数之一,对材料表层微观结构演变和综合性能具有十分重要的影响。因此,本文以2024-T351铝合金为研究对象,通过改变喷丸进给速度,研究喷丸覆盖率的变化对表面形貌、表面粗糙度、残余应力、微观硬度的影响规律。

1 材料及试验步骤

试验材料为2024-T351铝合金。在喷丸处理之前采用砂纸对试样进行抛光处理,砂纸目数依次为#400、#800、#1200、#2000、#4000。对抛光后的试样进行气动喷丸处理,喷丸处理的各项参数分别为陶瓷弹丸(型号AZB425)、弹丸直径0.425 mm、弹丸流量4 kg/min、喷丸气压0.25 MPa和喷丸距离300 mm。通过调节喷嘴的进给速度实现覆盖率的变化(喷丸覆盖率是指喷丸强化后,试样表面弹痕所占面积与总面积之比)。经过测量,喷嘴进给速度为2 m/min时,喷丸覆盖率为99.6%,因此以2 m/min的进给速度重复2次和4次喷

丸,对应的喷丸覆盖率分别为200%和400%。进给速度为4 m/min时,喷丸试样的覆盖率为88.3%。对应于88.3%、100%、200%及400%喷丸覆盖率的A型Almen试片弧高值分别为0.199 mm、0.223 mm、0.245 mm、0.253 mm。

使用Tescan Clara扫描电子显微镜(SEM)对原始和喷丸试样进行表面形貌观察,加速电压为15 kV。采用吉泰TR210表面粗糙度仪测量原始和喷丸试样的表面轮廓并计算表面粗糙度。使用Bruker D8 X射线衍射仪对原始和喷丸试样进行物相鉴定和微观结构分析。选用Cu靶 $K\alpha$ 辐射, 2θ 角范围为 $30^\circ\sim 80^\circ$,扫描速率 $2^\circ/\text{min}$ 。采用Jade 9.0软件进行XRD数据分析,选用高斯函数拟合各衍射峰^[37]。试样表层残余应力采用Proto iXRD便携式残余应力测试仪测量,测试条件为Co靶、电压20 kV、电流5 mA,测定Al(311)衍射峰。为获得沿深度分布的残余应力,采用化学腐蚀方法对试样进行剥层处理,腐蚀液选用质量分数为16.9%的NaOH溶液,温度为 80°C 。将原始和喷丸试样侧面进行抛光后,使用MHVS-1000Z维氏硬度计测量沿深度方向的硬度,载荷大小0.245 N、保载时间10 s,相邻测试点间距离为50 μm 。

2 试验结果与讨论

2.1 表面形貌及粗糙度

原始和喷丸试样的表面形貌如图1所示。图1(a)中的原始试样经过#4000砂纸打磨后,磨痕较浅且方向一致,试样表面光滑。从图1(b)可以看出,弹丸对试样表面的撞击使其产生了明显的弹痕,同时,弹痕之间重叠及挤压等相互作用导致相邻弹痕交界处的凸起。此时,试样表面仍然存在未喷丸区域。随着喷丸覆盖率增加至100%、200%、400%,试样表面被弹痕完全覆盖,未见原始试样表面的打磨痕迹,如图1(c)~(e)所示。然而,随着喷丸覆盖率的提高,试样表面逐渐出现褶皱、微裂纹等缺陷。覆盖率100%的喷丸试样表面(图1(c))已出现少量的褶皱^[37],覆盖率200%的喷丸试样表面的褶皱数量明显增加,覆盖率400%的喷丸试样在褶皱数量进一步增加的同时出现了微裂纹^[7]。Zhou等^[12]在气动喷丸和超声喷丸对比试验中指出,气动喷丸覆盖率的增加将导致微裂纹的产生。

原始及喷丸试样的表面轮廓曲线及表面粗糙度如图2所示。可以看出,经过抛光的原始试样表面光滑,试样喷丸前后表面轮廓曲线值(图2(a))与图1(a)所示的试样表面形貌基本一致,原始试样表面粗糙度 R_a 为0.144 μm 。由于弹丸的撞击,喷丸试样表面轮廓曲线高低起伏明显,且转角尖锐,因此喷丸试样的表面粗糙

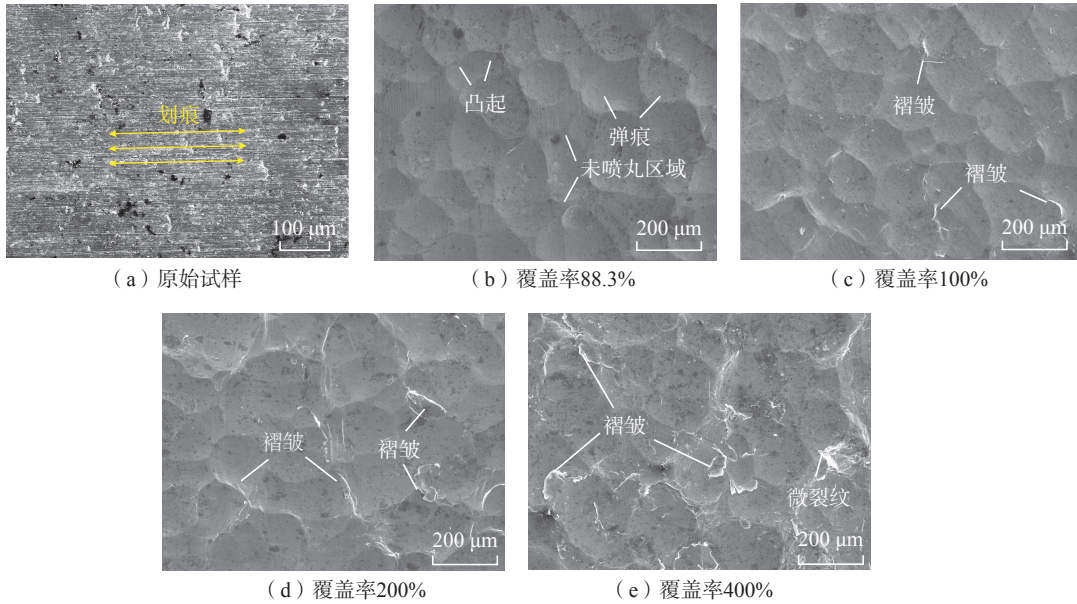


图1 原始试样及不同覆盖率喷丸试样的表面形貌
Fig.1 Surface morphology of initial and shot peened samples with different coverage

度显著增加,覆盖率 88.3%、100%、200% 和 400% 的喷丸试样表面粗糙度 R_a 分别为 $4.263 \mu\text{m}$ 、 $4.601 \mu\text{m}$ 、 $4.090 \mu\text{m}$ 、 $4.052 \mu\text{m}$ 。如图 2(b)所示,随着喷丸覆盖率的增加,喷丸试样的表面粗糙度 R_a 先增加后减小。当喷丸覆盖率为 88.3% 时,弹痕未完全覆盖试样表面,喷丸试样表面粗糙度增加但未到最大值。随着喷丸覆盖率增加,弹痕之间的相互作用逐渐加剧,导致表面粗糙度的进一步提高,当覆盖率为 100% 时喷丸试样表面粗糙度最大。然而,后续弹丸的撞击减小了凸起区域的高度,在弹痕轮廓变得模糊的同时,表面粗糙度下降。因此,覆盖率为 200% 的喷丸试样表面粗糙度降低。同时,大量弹丸的多次撞击也导致褶皱出现的频率增加。而当覆盖率进一步增加时,后续弹丸对试样表面的撞击将进一步减小表面轮廓的高度差,因此覆盖率为 400% 的喷丸试样表面轮廓曲线的波动程度显著减小。然而,由于过高的喷丸覆盖率,试样表面的褶皱数量显著增加。同时,由于塑性应变的累积超过了材料的强度极限,导致微裂纹的产生,这将显著降低材料的服役性能。

2.2 XRD 分析

原始和喷丸试样的 XRD 图谱及其半峰全宽 (FWHM) 如图 3 所示。通过与标准 XRD 数据 (ICCD PDF 编号 01-085-1327) 对比,喷丸前后 2024-T351 铝合金试样的物相保持不变。然而,喷丸处理导致衍射峰的宽化。图 3 (b) 所示为 Al (111)、Al (200)、Al (220) 的 FWHM 随喷丸覆盖率的变化规律,可以看出相比于原始试样,喷丸引起衍射峰的宽化,且随喷丸覆盖率的增加,各衍射峰的 FWHM 逐渐增大。X 射线衍射峰的宽

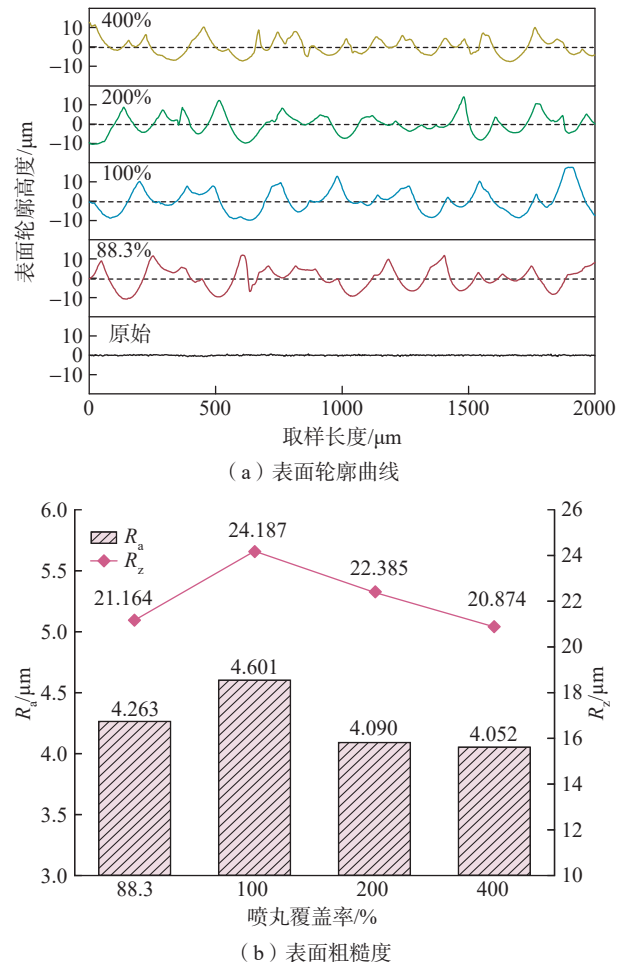


图2 原始及喷丸试样的表面轮廓曲线和表面粗糙度
Fig.2 Surface contours and surface roughness of initial and shot peened samples

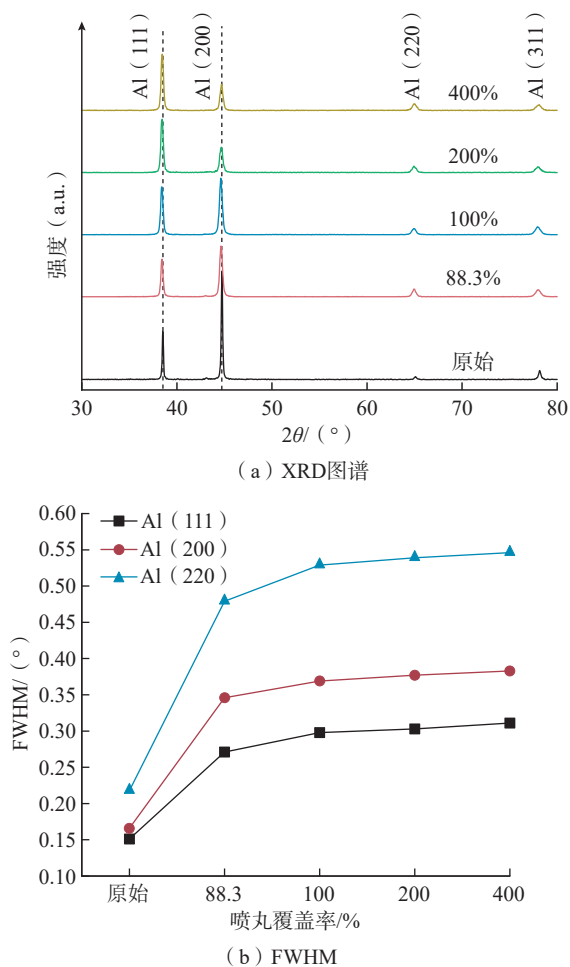


图3 原始试样与不同喷丸覆盖率试样的 XRD 图谱及 FWHM
Fig.3 XRD patterns and FWHM of initial and shot peened samples with various coverage

度包括仪器宽度和结构展宽两部分,二者满足卷积关系^[38]。而结构展宽由晶粒细化和微观应变的增加导致。因此,晶粒尺寸和微观应变可用式(1)计算^[1,39]:

$$\beta_h^2 - \beta_0^2 = \frac{\lambda}{D_h \cos\theta} + (4\varepsilon \tan\theta)^2 \quad (1)$$

式中, β_h 为衍射峰的 FWHM; β_0 为仪器宽度; λ 为入射线波长; D_h 为微晶尺寸; θ 为入射角; ε 为微观应变。经过计算,原始试样和覆盖率为 88.3%、100%、200%、400% 的喷丸试样微晶尺寸分别为 338 nm 和 246 nm、218 nm、178 nm、166 nm。相应的微观应变分别为 0.045、0.289、0.313、0.341、0.377。由于微晶尺寸均大于 100 nm,喷丸试样的衍射峰宽化归因于微观应变的增加^[10]。同时可以看出,微晶尺寸随喷丸覆盖率的增加而减小,而微观应变随喷丸覆盖率增加而增大。这与喷丸过程中的塑性变形有关,喷丸覆盖率的增加导致更加剧烈的塑性变形,进一步诱发位错增殖及晶粒细化等。Liu 等^[19]研究也指出喷丸时间的延长将产生更加显著的加工硬

化和晶粒细化。

2.3 残余应力

图 4 为原始试样和喷丸试样的残余应力场。原始试样中几乎不存在残余应力。试样经过喷丸处理后,不同覆盖率试样表面均产生残余压应力场。残余压应力沿深度方向先增大后逐渐减小。喷丸过程中,大量、高速弹丸的撞击使材料表面产生塑性变形层,其膨胀变形的趋势被周围材料的弹性响应抑制,在喷丸表面产生了残余压应力。而残余压应力最大值所在位置影响因素较多。Feng 等^[40]研究喷丸强化双相不锈钢的残余应力分布,指出奥氏体中残余应力最大值出现在次表层,而铁素体中的残余应力最大值出现在表层。Li 等^[41]指出,残余压应力的数值与位错密度有关。表层的位错湮灭和重排导致残余压应力数值减小,因此残余压应力最大值位于次表层。Feng 等^[42]认为 Hertz 动态压缩与塑性延展的竞争机制决定了残余压应力场的分布,当 Hertz 动态压缩占主导地位时,残余应力最大值出现在次表面^[43]。

残余压应力场可由 4 个特征参数确定:表面残余压应力、残余压应力最大值、残余压应力最大值所在深度、残余压应力层深度^[42]。如图 4 所示,残余压应力场的特征参数总体上随喷丸覆盖率的增加而增大。然而,覆盖率 400% 的喷丸试样表面残余压应力为 -337.9 MPa,小于覆盖率 200% 喷丸试样的 -344.0 MPa,可能与 400% 覆盖率试样产生表面褶皱及微裂纹有关^[7]。覆盖率 88.3%、100%、200%、400% 的喷丸试样残余压应力最大值分别为 -346.4 MPa、-364.1 MPa、-378.2 MPa、-385.6 MPa,随喷丸覆盖率的增加而增大。残余压应力最大值所在深度及残余压应力层深度随覆盖率的增加显著增加,覆盖率 88.3%、100%、200%、400% 的喷丸试样残余压应力层深度分别为 176.5 μm 、190.2 μm 、201.5 μm 、210.5 μm 。随着喷丸覆盖率的增大,塑性变形层沿深度方向扩展,弹性响应的区域随之扩大,因此残余压应力

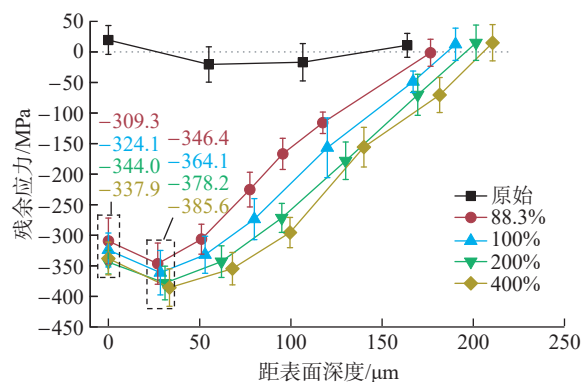


图4 原始及喷丸试样残余应力场
Fig.4 Residual stress field of initial and shot peened samples

层深度显著增大。

2.4 微观硬度

原始试样和喷丸试样沿深度方向的维氏硬度曲线如图 5 (a) 所示。原始试样的微观硬度稳定在 $160\text{HV}_{0.025}$ 附近。气动喷丸后,试样表层微观硬度均明显增加,最大值出现在试样表面,并沿深度方向逐渐减小至基体硬度。同时,随喷丸覆盖率的增加,微观硬度最大值和硬化层深度明显增大。图 5 (b) 为微观硬度最大值和硬化层深度随喷丸覆盖率的变化趋势。相比于原始试样,覆盖率 88.3%、100%、200%、400% 的喷丸试样微观硬度分别增加了 18.4%、22.8%、25.1% 和 27.2%。材料的强化机制包括细晶强化、应变强化、第二相强化和固溶强化 4 种方式。如 2.2 节所述,在喷丸过程中,高速弹丸的撞击引起了试样表面细化和微应变增加,使试样微观硬度增加^[19]。同时,由于应变和应变速率随深度的增加而减小,晶粒细化程度和位错密度同时降低^[43],形成了沿深度方向的梯度结构^[20,22],因此喷丸试样的硬

度值沿深度逐渐减小。随着覆盖率的增加,试样表面的晶粒更加细化,微应变显著增大,因此微观硬度上升。

3 结论

本文研究了喷丸覆盖率对 2024-T351 铝合金的表面完整性的影响,主要结论如下。

(1) 表面粗糙度随喷丸覆盖率的增加先增大后减小。覆盖率 100% 的喷丸试样表面粗糙度最大 ($R_a=4.601\mu\text{m}$)。随着覆盖率增加,喷丸试样表面褶皱数量增多。覆盖率 400% 的喷丸试样表面出现大量的褶皱,且形成了微裂纹。

(2) 喷丸试样表面存在残余压应力场。随喷丸覆盖率的提高,残余压应力最大值、残余压应力场深度逐渐增大。

(3) 喷丸引起试样微观硬度的提高。喷丸覆盖率的增大促进了微观硬度的提高及硬化层深度的增加。

参考文献

[1] SUN Q Q, LIU X T, HAN Q Y, et al. A comparison of AA2024 and AA7150 subjected to ultrasonic shot peening: Microstructure, surface segregation and corrosion[J]. Surface and Coatings Technology, 2018, 337: 552-560.

[2] ALHAMIDI A, HORITA Z. Grain refinement and high strain rate superplasticity in aluminium 2024 alloy processed by high-pressure torsion[J]. Materials Science and Engineering: A, 2015, 622: 139-145.

[3] LIU Z, CHONG P H, BUTT A N, et al. Corrosion mechanism of laser-melted AA 1014 and AA 2024 alloys[J]. Applied Surface Science, 2005, 247(1-4): 294-299.

[4] KUMAR P, MAHOBIA G S, MANDAL S, et al. Enhanced corrosion resistance of the surface modified Ti-13Nb-13Zr alloy by ultrasonic shot peening[J]. Corrosion Science, 2021, 189: 109597.

[5] 胡英俊, 黄小波, 高玉魁. 喷丸处理对铝合金微动磨损及抗腐蚀性能的影响[J]. 表面技术, 2020, 49(7): 238-244, 254.

HU Yingjun, HUANG Xiaobo, GAO Yukui. Effect of shot peening on fretting wear and corrosion resistance of zirconium alloy[J]. Surface Technology, 2020, 49(7): 238-244, 254.

[6] ZHANG J Y, PENG P, SHE J, et al. A study of the corrosion behavior of AZ31 Mg alloy in depth direction after surface nanocrystallization[J]. Surface and Coatings Technology, 2020, 396: 125968.

[7] QIN Z, LI B, ZHANG H, et al. Effects of shot peening with different coverage on surface integrity and fatigue crack growth properties of 7B50-T7751 aluminum alloy[J]. Engineering Failure Analysis, 2022, 133: 106010.

[8] LI J, ZHOU J Z, FENG A X, et al. Analysis of microstructure and tensile properties produced by cryogenic laser peening on 2024-T351 aluminum alloy[J]. Vacuum, 2018, 158: 141-145.

[9] HU Y X, CHENG H, YU J H, et al. An experimental study on crack closure induced by laser peening in pre-cracked aluminum alloy

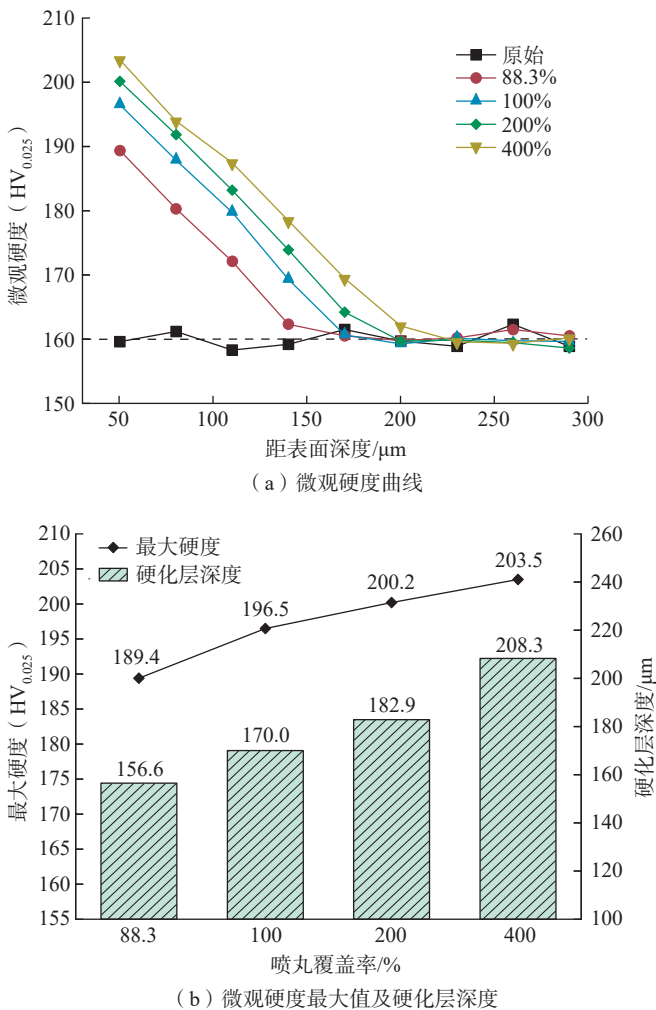


图 5 原始试样和喷丸试样的微观硬度

Fig.5 Microhardness of initial and peened samples

2024-T351 and fatigue life extension[J]. *International Journal of Fatigue*, 2020, 130: 105232.

[10] ZHANG Q, DUAN B B, ZHANG Z Q, et al. Effect of ultrasonic shot peening on microstructure evolution and corrosion resistance of selective laser melted Ti-6Al-4V alloy[J]. *Journal of Materials Research and Technology*, 2021, 11: 1090-1099.

[11] SOYAMA H, CHIGHIZOLA C R, HILL M R. Effect of compressive residual stress introduced by cavitation peening and shot peening on the improvement of fatigue strength of stainless steel[J]. *Journal of Materials Processing Technology*, 2021, 288: 116877.

[12] ZHOU J, RETRAINT D, SUN Z, et al. Comparative study of the effects of surface mechanical attrition treatment and conventional shot peening on low cycle fatigue of a 316L stainless steel[J]. *Surface and Coatings Technology*, 2018, 349: 556-566.

[13] MALEKI E, UNAL O, GUAGLIANO M, et al. The effects of shot peening, laser shock peening and ultrasonic nanocrystal surface modification on the fatigue strength of Inconel 718[J]. *Materials Science and Engineering: A*, 2021, 810: 141029.

[14] MASAYOSHI K, CURD MATTHEW E, HITOSHI S, et al. Depth-profiling of residual stress and microstructure for austenitic stainless steel surface treated by cavitation, shot and laser peening[J]. *Materials Science & Engineering A*, 2021, 813: 141037.

[15] YANG C, LI M Q, LIU Y G. Further refinement mechanisms of nanograins in nanocrystalline surface layer of TC17 subjected to severe plastic deformation[J]. *Applied Surface Science*, 2021, 538: 147941.

[16] SUN Q Q, HAN Q Y, LIU X T, et al. The effect of surface contamination on corrosion performance of ultrasonic shot peened 7150 Al alloy[J]. *Surface and Coatings Technology*, 2017, 328: 469-479.

[17] WANG H T, YAO H L, ZHANG M X, et al. Surface nanocrystallization treatment of AZ91D magnesium alloy by cold spraying shot peening process[J]. *Surface and Coatings Technology*, 2019, 374: 485-492.

[18] XU G, LUO K Y, DAI F Z, et al. Effects of scanning path and overlapping rate on residual stress of 316L stainless steel blade subjected to massive laser shock peening treatment with square spots[J]. *Applied Surface Science*, 2019, 481: 1053-1063.

[19] LIU Y G, LI H J, LI M. Roles for shot dimension, air pressure and duration in the fabrication of nanocrystalline surface layer in TC17 alloy via high energy shot peening[J]. *Journal of Manufacturing Processes*, 2020, 56: 562-570.

[20] LIU Y G, LI M Q, LIU H J. Surface nanocrystallization and gradient structure developed in the bulk TC4 alloy processed by shot peening[J]. *Journal of Alloys and Compounds*, 2016, 685: 186-193.

[21] LI H M, LIU Y G, LI M Q, et al. The gradient crystalline structure and microhardness in the treated layer of TC17 via high energy shot peening[J]. *Applied Surface Science*, 2015, 357: 197-203.

[22] AO N, LIU D X, XU X C, et al. Gradient nanostructure evolution and phase transformation of α phase in Ti-6Al-4V alloy induced by ultrasonic surface rolling process[J]. *Materials Science and Engineering: A*, 2019, 742: 820-834.

[23] AO N, LIU D X, ZHANG X H, et al. Surface nanocrystallization of body-centered cubic beta phase in Ti-6Al-4V alloy subjected to

ultrasonic surface rolling process[J]. *Surface and Coatings Technology*, 2019, 361: 35-41.

[24] 杨诗婷, 邢永明, 郎凤超, 等. 喷丸强化 316L 不锈钢表面的摩擦磨损性能 [J]. *金属热处理*, 2016, 41(11): 35-39.

YANG Shiting, XING Yongming, LANG Fengchao, et al. Friction and wear properties of 316L stainless steel after shot peening[J]. *Heat Treatment of Metals*, 2016, 41(11): 35-39.

[25] 蔡雨晴, 胡雄风, 屈盛官, 等. 喷丸强化对 CF53 钢摩擦磨损性能的影响 [J]. *机械工程材料*, 2021, 45(5): 27-33, 38.

CAI Yuqing, HU Xiongfeng, QU Shengguan, et al. Effect of shot peening on friction and wear properties of CF53 steel[J]. *Materials for Mechanical Engineering*, 2021, 45(5): 27-33, 38.

[26] ZHANG J Y, JIAN Y X, ZHAO X Z, et al. The tribological behavior of a surface-nanocrystallized magnesium alloy AZ31 sheet after ultrasonic shot peening treatment[J]. *Journal of Magnesium and Alloys*, 2021, 9(4): 1187-1200.

[27] ZHANG Y L, LAI F Q, QU S G, et al. Effect of shot peening on residual stress distribution and tribological behaviors of 17Cr2Ni2MoVnB steel[J]. *Surface and Coatings Technology*, 2020, 386: 125497.

[28] KLUMPP A, RUF M, DIETRICH S, et al. Long crack propagation and closure in DC(T) specimens of Ni-based superalloy Inconel 718 and stainless steel AISI 301 after shot peening[J]. *Engineering Fracture Mechanics*, 2022, 269: 108551.

[29] 孟宪凯, 张正焯, 周建忠, 等. 激光喷丸强化 TC6 钛合金的振动疲劳寿命及断口形貌分析 [J]. *航空制造技术*, 2022, 65(4): 73-79.

MENG Xiankai, ZHANG Zhengye, ZHOU Jianzhong, et al. Analysis of vibration fatigue life and fracture topography of TC6 titanium alloy by laser peening[J]. *Aeronautical Manufacturing Technology*, 2022, 65(4): 73-79.

[30] 黄舒, 胡磊, 盛杰, 等. 激光喷丸强化对电化学充氢 316L 奥氏体不锈钢振动疲劳性能的影响 [J]. *稀有金属材料与工程*, 2022, 51(2): 579-587.

HUANG Shu, HU Lei, SHENG Jie, et al. Effect of laser peening on vibration fatigue performance of electrochemically hydrogen-charged 316L austenitic stainless steel[J]. *Rare Metal Materials and Engineering*, 2022, 51(2): 579-587.

[31] 王成, 李开发, 胡兴远, 等. 喷丸强化残余应力对 AISI 304 不锈钢疲劳裂纹扩展行为的影响 [J]. *表面技术*, 2021, 50(9): 81-90, 151.

WANG Cheng, LI Kaifa, HU Xingyuan, et al. Effects of shot peening-induced residual stresses on fatigue crack propagation behavior of AISI 304 stainless steel[J]. *Surface Technology*, 2021, 50(9): 81-90, 151.

[32] LUO X K, WANG Y M, DANG N, et al. Gradient microstructure and foreign-object-damaged fatigue properties of Ti6Al4V titanium alloy processed by the laser shock peening and subsequent shot peening[J]. *Materials Science and Engineering: A*, 2022, 849: 143398.

[33] FERREIRA N, JESUS J S, FERREIRA J A M, et al. Effect of bead characteristics on the fatigue life of shot peened Al7475-T7351 specimens[J]. *International Journal of Fatigue*, 2020, 134: 105521.

[34] YANG S, ZENG W, YANG J S. Characterization of shot

peening properties and modelling on the fatigue performance of 304 austenitic stainless steel[J]. *International Journal of Fatigue*, 2020, 137: 105621.

[35] GAO T, SUN Z D, XUE H Q, et al. Effect of surface mechanical attrition treatment on high cycle and very high cycle fatigue of a 7075-T6 aluminium alloy[J]. *International Journal of Fatigue*, 2020, 139: 105798.

[36] LIU Z G, WONG T I, HUANG W, et al. Effect of surface polishing treatment on the fatigue performance of shot-peened Ti-6Al-4V alloy[J]. *Acta Metallurgica Sinica (English Letters)*, 2017, 30(7): 630-640.

[37] ZHANG Q, XU S, ZHANG Z Q, et al. Residual stress and microhardness evolution induced by conventional and ultrasonic shot peening[J]. *Materials Science and Technology*, 2022, 38(7): 436-443.

[38] WILLIAMSON G K, HALL W H. X-ray line broadening from filed aluminium and wolfram[J]. *Acta Metallurgica*, 1953, 1(1): 22-31.

[39] SUN Q Q, HAN Q Y, XU R, et al. Localized corrosion behaviour of AA7150 after ultrasonic shot peening: Corrosion depth vs. impact energy[J]. *Corrosion Science*, 2018, 130: 218-230.

[40] FENG Q, WU X Y, JIANG C H, et al. Surface layer investigation of a shot-peened duplex stainless steel utilizing X-ray diffraction[J]. *Journal of Materials Engineering and Performance*, 2013, 22(7): 2005-2011.

[41] LI K, FU X S, LI R D, et al. A mechanism study on characteristic curve of residual stress field in Ti-6Al-4V induced by wet peening treatment[J]. *Materials & Design*, 2015, 86: 761-764.

[42] FENG B X, MAO X N, YANG G J, et al. Residual stress field and thermal relaxation behavior of shot-peened TC4-DT titanium alloy[J]. *Materials Science and Engineering: A*, 2009, 512(1-2): 105-108.

[43] FU P, JIANG C H, WU X Y, et al. Surface modification of 304 steel using triple-step shot peening[J]. *Materials and Manufacturing Processes*, 2015, 30(6): 693-698.

通讯作者: 徐刚, 高级工程师, 研究方向为大型金属零件喷丸加工技术。

(责编 晓月)

(上接第 105 页)

[25] HE H T, SHAO G, ZHAO R, et al. Effects of oscillatory pressure mode on the sintering behavior of Al_2O_3 - ZrO_2 composite in hot oscillatory pressing[J]. *Journal of the American Ceramic Society*, 2022, 105(12): 7778-7784.

[26] ZHANG J, ZHU T B, CHENG Y, et al. Fabrication and mechanical properties of ZrO_2 - Al_2O_3 -SiC(w) composites by oscillatory pressure sintering[J]. *Ceramics International*, 2020, 46(16): 25719-25725.

[27] ZHU T B, XIE Z P, HAN Y, et al. Improved mechanical properties of Al_2O_3 -25vol% SiC_w composites prepared by oscillatory pressure sintering[J]. *Ceramics International*, 2017, 43(17): 15437-15441.

[28] ZHU T B, XIE Z P, HAN Y, et al. Microstructure and mechanical properties of ZTA composites fabricated by oscillatory

pressure sintering[J]. *Ceramics International*, 2018, 44(1): 505-510.

[29] HAN Y, LI S, ZHU T B, et al. Enhanced toughness and reliability of Si_3N_4 -SiC_w composites under oscillatory pressure sintering[J]. *Ceramics International*, 2018, 44(11): 12169-12173.

[30] YANG S L, ZHU Y X, FAN L, et al. Preparation and mechanical properties of SiC_w- Al_2O_3 -YAG ceramic composite by hot oscillatory pressing[J]. *Ceramics International*, 2021, 47(15): 21231-21235.

[31] SHAHEDI ASL M, GHASSEMI KAKROUDI M, GOLESTANI-FARD F, et al. A Taguchi approach to the influence of hot pressing parameters and SiC content on the sinterability of ZrB_2 -based composites[J]. *International Journal of Refractory Metals and Hard Materials*, 2015, 51: 81-90.

[32] LIU D G, FAN J Y, ZHAO K, et al. Preparation of super-strong ZrO_2 ceramics using dynamic hot forging[J]. *Journal of the European Ceramic Society*, 2023, 43(2): 733-737.

[33] ZHAO K, FENG P, TAN J, et al. A new route to fabricate high-performance binderless tungsten carbide: Dynamic sinter forging[J]. *Journal of the American Ceramic Society*, 2023, 106(6): 3343-3350.

[34] FAN L, SONG X W, ZHAO P F, et al. Super strong B_4C ceramics prepared by dynamic sinter forging[J]. *Journal of the European Ceramic Society*, 2023, 43(9): 4209-4214.

[35] ZHU T B, XIE Z P. Ultrastrong tough zirconia ceramics by defects-engineering[J]. *Journal of the American Ceramic Society*, 2022, 105(3): 1617-1621.

[36] ZHOU P, HU P, ZHANG X H, et al. R-curve behavior of laminated ZrB_2 -SiC ceramic with strong interfaces[J]. *International Journal of Refractory Metals and Hard Materials*, 2015, 52: 12-16.

[37] ZHU S M, FAHRENHOLTZ W G, HILMAS G E. Influence of silicon carbide particle size on the microstructure and mechanical properties of zirconium diboride-silicon carbide ceramics[J]. *Journal of the European Ceramic Society*, 2007, 27(4): 2077-2083.

[38] ZHOU P, HU P, ZHANG X H, et al. Laminated ZrB_2 -SiC ceramic with improved strength and toughness[J]. *Scripta Materialia*, 2011, 64(3): 276-279.

[39] WEI C C, ZHANG Z Y, MA X F, et al. Mechanical and ablation properties of laminated ZrB_2 -SiC ceramics with Si_3N_4 whisker interface[J]. *Corrosion Science*, 2022, 197: 110051.

[40] LÜ Z H, JIANG D L, ZHANG J X, et al. ZrB_2 -SiC laminated ceramic composites[J]. *Journal of the European Ceramic Society*, 2012, 32(7): 1435-1439.

[41] FANG X, BISHARA H, DING K, et al. Nanoindentation pop-in in oxides at room temperature: Dislocation activation or crack formation?[J]. *Journal of the American Ceramic Society*, 2021, 104: 4728-4741.

[42] XU H Y, JI W, GUO W M, et al. Enhanced mechanical properties and oxidation resistance of zirconium diboride ceramics via grain-refining and dislocation regulation[J]. *Advanced Science*, 2022, 9(6): e2104532.

通讯作者: 刘金铃, 教授, 博士, 研究方向为材料场辅助制造技术、陶瓷基复合材料、金属基复合材料和材料强韧化机理。

(责编 晓月)